Evaporation induced property change and hidden cavity formation

Iltai (Isaac) Kim
School of Engineering and Computing Science
Texas A&M University-Corpus Christi, Corpus Christi, TX ikim@tamucc.edu

ABSTRACT

Innovative optical techniques based on nano-biophotonics such as surface plasmon resonance (SPR) imaging are developed to characterize the transport and optical properties of nanofluids in situ, real-time, and full field manner. 47 nm Al2O3 nanoparticles are dispersed in water with various concentrations. Al2O3 nanofluids droplets are placed on substrates and evaporated in room temperature. Simultaneous surface Plasmon resonance imaging and natural fringe mapping techniques are employed to characterize solid-liquid-vapor phases of nanofluids during self assembly process in real-time and full-field manner. During the evaporation, time-dependent and near-field nanoparticle concentrations are determined by correlating the SPR reflectance intensities with the effective refractive index (ERI) of the nanofluids. Furthermore, the existence of hidden complex cavities formed inside a self-assembled nanocrystalline structure is discovered in real-time. R-G-B interference fringes allowed us to reconstruct the 3D cavity formation and crystallization processes quantitatively. The formation of the complex inner structure was found to be attributable to multiple cavity inceptions and their competing growth during the aquatic evaporation. Additionally, the effect of surface hydrophobicity is examined in the formation of hidden complex cavities during the evaporation-induced nanocrystalline self-assembly, taking place on three different substrates bearing different levels of hydrophobicity; namely, cover glass (CG), gold thin film (Au), and polystyrene dish (PS).

These surface plamson resonance imaging and natural fringe mapping techniques are expected to provide substantial tools to characterize nano-bio materials and their interaction phenomena when coupled with localized surface Plasmon and hyperbolic metamaterials.

Keywords: surface plasmon resonance, self-assembly, hydrophobicity

Introduction

Nanofluids and nanoparticle crystalline structure are attracting increasing attention because of the important applications, including heat transfer enhancement, nanoscale manufacturing, and bio-process [1-5]. Several techniques have been developed to characterize the physical and optical properties of nanofluids up to date [3, 6-12]. Recently, innovative optical techniques based on nano-biophotonics such as surface plasmon resonance (SPR) imaging and R-G-B natural fringe mapping techniques are developed and demonstrated to characterize the transport and optical properties of nanofluids in situ, real-time, and full field manner [13-17]. In this paper, recent achievements regarding evaporation-induced trasnport property change and cavity formation will be summarized and future research direction will be discussed.

Simultaneous SPR and Fringe mapping

The present in-situ visualization experiments were conducted with an aqueous solution containing various concentrations (0.1 ~ 12 %) of 47-nm average diameter Al_2O_3 nanoparticles (Fig. 1); the solution is laid on a gold surface at a constant humidity of 40% and a laboratory temperature of 21±0.5°C. No surfactant or additives were used in sonically mixing the 47-nm Al_2O_3 nanoparticles with deionized water at the authors' laboratory. Note that he 47-nm diameter is an average value for the inevitably distributed Al_2O_3 nanoparticles. Fig. 1 shows a simultaneous optical system to image both dorsal and ventral views of the evaporation-induced self-assembly phenomena of nanofluids at the same time. Normal optical reflected widefield microscopy (WFM) is used for dorsal view imaging from the top. The *SPR* imaging identifies the near-surface phenomena like the existence of hidden cavity structures viewed from the bottom, and the quantitative analysis of *R-G-B* natural fringes [20] delineates the complex inner dimensions of the three-dimension cavity [17].

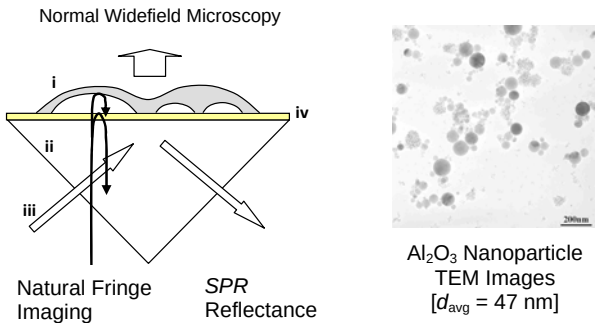

Figure 1. Hybrid optical system of dorsal view from the top, *SPR* imaging, and natural fringe view of the evaporation-induced cavity structure at the Al_2O_3 concentration of 10% (i). The prism (ii) creates the evanescent wave field under total internal reflection conditions when illuminated with *p*-polarized monochromatic light (iii). The free electrons in the 47.5-nm thick Au thin film (iv) [12, 17].

The schematic of *SPR* is illustrated in Fig. 2, which shows

the Kreschtmann's principle of *SPR* occurring at

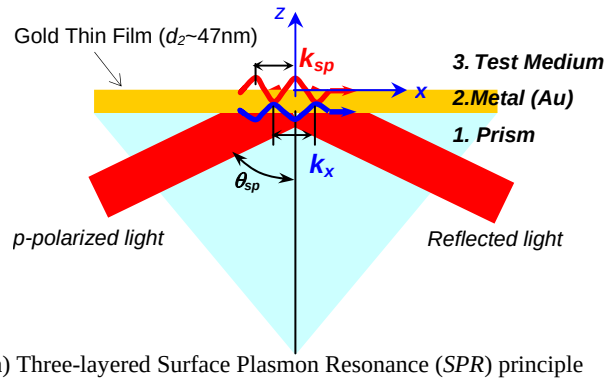

(a) Three-layered Surface Plasmon Resonance (*SPR*) principle

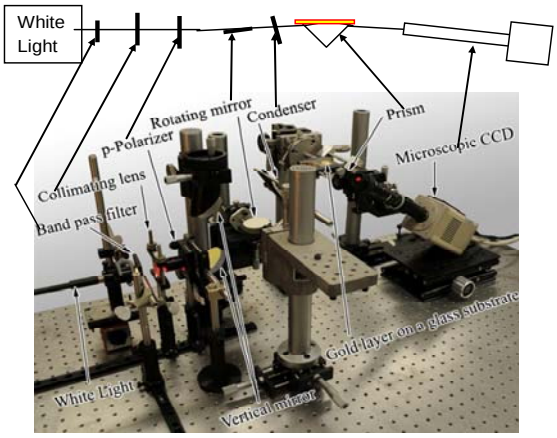

(b) The optical train for *SPR* generation and detection of its reflectance intensity

Figure 2. Surface Plasmon Resonance (*SPR*) system: (a) Kreschmann configuration of a three-layered *SPR* principle, where the glass prism, the metallic gold film and the test medium are labeled 1, 2 and 3, respectively, and (b) the experimental layout of the *SPR* imaging system using a *p*-polarized white light source [15, 18].

the interface of a thin-layered metal film contacting the external test medium [15, 18, 19]. When a thin metal film is illuminated by a coherent p-polarized light at an incident angle exceeding the critical angle for total internal reflection, the evanescent wave vector ($\vec{k}_x$) is formed at the incident (bottom) metal surface that successively triggers coherent fluctuations of free electrons at the surface of the metal film. This coherent energy conversion of the photons into free electrons is called the Surface Plasmon (SP) phenomenon. The resonant excitation of SP in the laterally heterogeneous interface occurs when the condition of momentum matching is fulfilled, i.e., $\vec{k}_x = \vec{k}_{sp}$ where $\vec{k}_x$ is the evanescent wave vector along the surface. When the SP waves penetrate into the very thin metal film and collectively oscillate to form amplified waves, the SPR wave is achieved on the emitting (top) surface of the metal layer [19].

Effective refractive index mapping using SPR

Effective refractive index of nanofluids is successfully measured through total internal reflection (TIR) and verified using SPR reflectance imaging as in Fig. 3 [16]. Firstly, effective refractive index (ERI) is determined from TIR experiment and its measurement is in quite good agreement with Rayleigh scattering theory. Then experimental correlation for ERI is obtained between SPR reflectance and ERI to show that SPR imaging can successfully measure ERI of nanofluids.

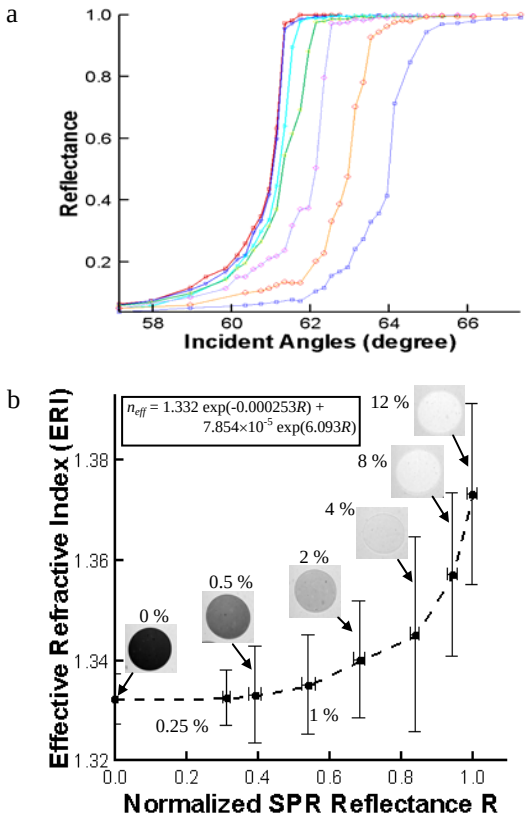

Figure 3. (a) Experimental determination of ERI of nanofluids using TUR and (b) correlation of TIR with normalized SPR reflectance *R* for varying concentrations [16].

Fig. 4 shows in-situ visualization of evaporation-induced self-assembly process at the low concentration of 0.25 % using SPR imaging [16]. It presents in-situ visualization of varying nanofluids concentration and its corresponding effective refractive index (ERI) of evaporating nanofluids. The dry-out pattern shows the traditional pattern of coffee ring that self-finning occurs along the edge of droplets. SPR imaging technique shows that it can detect optical property variation of effective refractive index in label-free and quantitative manner.

With increasing concentration, the dry-out pattern shows very exciting features as in Fig. 5-b. At first time when this dramatic patterns in SPR imaging were observed, it was not clearly understood what the white intensity stands for. The samples of self-assembly pattern happened

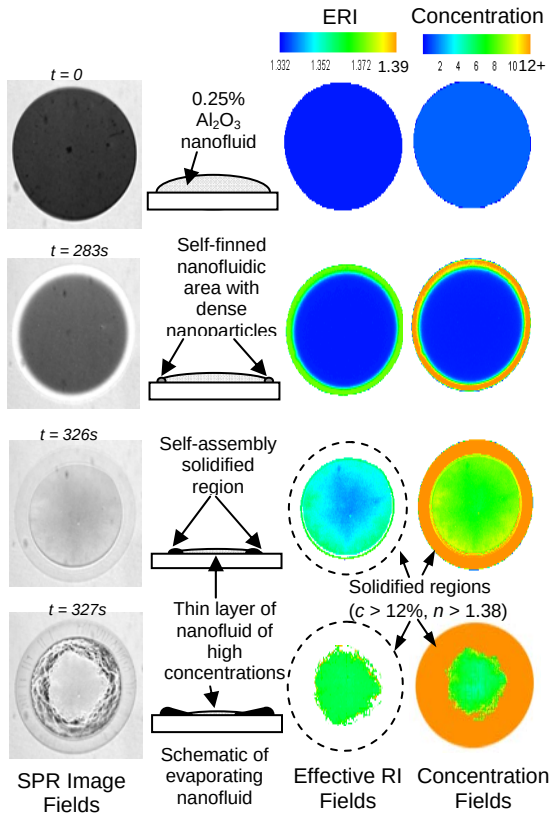

Figure 4 Full-field and real-time mapping of effective refractive index (ERI) and volume concentration distributions [16].

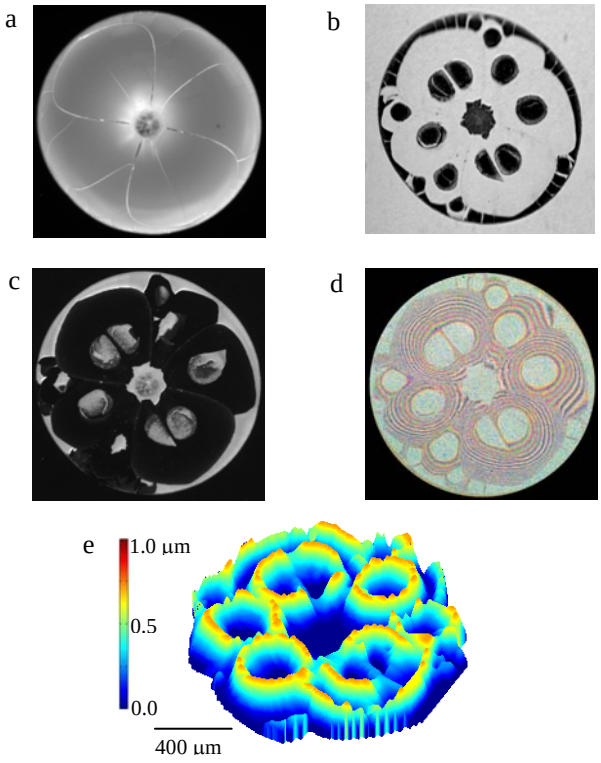

Figure 5. Self-assembled nanocrystalline structure revealing the hidden hollow complex cavities at the concentration of 10% Al_2O_3 nanoparticles. (a) The normal widefield microscopic dorsal view shows the crystallized half-toroidal glassy surface of approximately 2.0-mm diameter and 160-μm maximum height. (b) Nonintrusive near-field *SPR* imaging clearly shows the existence of the hidden hollow cavity structures. (c) The destructive image taken with the roof shattered confirms the *SPR* image. (d) Natural fringe *R-G-B* interference map is constructed by incident ray interference when they are reflected from both the ventral inner cavity surface and the gold surface, which carry quantitative information on the cavity dimensions. (e) Three-dimensional reconstruction of the *R-G-B* fringe map from the computer analysis of (d) [17].

to be impacted such that the top layer was removed. The destructively opened view clearly shows that the white region have no nanoparticles attached on the surface (Fig. 5); cavity is formed under the nanocrystalline structure! SPR images map the evolution of near-field cavity structures by means of intensity difference among the vapor (gray), liquid (white), and solid (black) phases simultaneously. Thus, the natural fringe R-G-B mapping technique was employed to estimate the magnitude of cavity [17].

The three-dimensional reconstruction image (Fig. 5-e) unveils the hidden complex cavity structures and completes the detailed 3-D topography showing the maximum vertical scale of 0.72 μm while the maximum crest roof thickness reaches 160 μm. With improvement in sensitivity and localized SPR technique [23] based on nano-biophotonics, it is expected to detect the vortex motion of nanofluids during the evaporation process.

The dry-out pattern of nanofluids also shows hallow cavity formation at the lower concentration of 1.25% using natural fringe mapping when nanofluids droplets are put on hydrophilic, less hydrophillic, and hydrophobic substrates such as glass slide, gold (Au) and polystyrene (PS) dish [13, 14] as in Fig. 6. The general dorsal view using optical microscope doesn't detect any cavity formation inside the nanocrystalline structure. It shows dramatic dry-out pattern formation difference depending on the surface hydrophobicies [14]. Also note that the effective time that cavities are generated is shorter in hydrophobic surface of polystyrene dish than in hydrophilic surface of glass slide by one seventh, which is estimated to be larger DLVO forces on the hydrophillic surface than the hydrophobic one.

Summary

Recent research achievement shows that there are still various factors we need to address to clearly understand the

self-assembly phenomena of nanofluids, which is basically similar to nature materials. Future effort is required on the formation of nanaocavity with controlled experiments such as the relative thermal conductance between the nanofluids and the substrate surface, the surface energy (hydrophobicities), and nanoparticle size

effects. Furthermore, it is expected to visualize to individual particle's motion when metal nanoparticles are mixed with

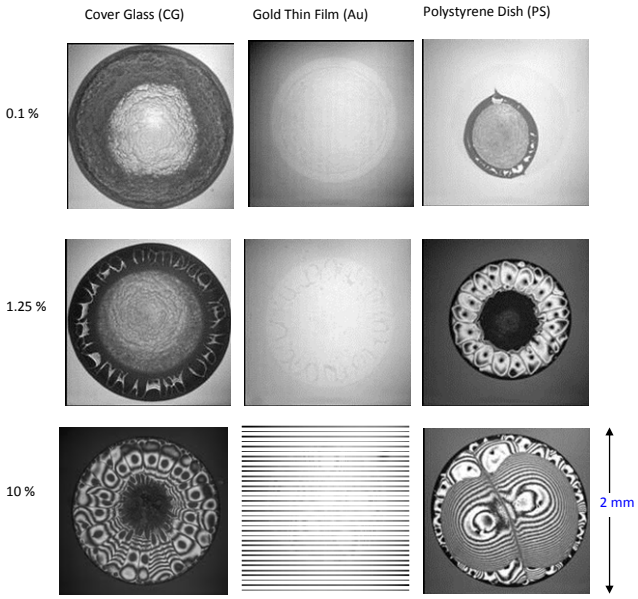

Figure 6. Microscopic ventral view images (natural fringe imaging) of hidden complex cavities of Al_2O_3 nanofluids of three different initial volume concentrations on three different substrates with increasing hydrophobicity: cover glass (CG), gold thin film (Au), and polystyrene dish (PS). Concentration is 1.25 %. [14].

nanofluids using SPR emission mode [21, 23].

Other unresolved issues in the optical characterization of nanofluids are the effective refractive index at high concentrations during the evaporation process [16] and the change of optical property during the solidification of nanofluids [17]. The approach of higher refractive index prism, tunable SPR resonance wavelength, and enhanced sensitivity is expected to address these issues [24].

References

[1] N. Sing and D. Banerjee, "Nanofins: Science and applications", Springer, New York, N.Y. 2014.

[2] S.U.S. Choi and J.A. Eastman, Enhancing thermal conductivity of fluids with nanoparticles, in: Conference: International Mechanical Eengineering Congress and Exhibition, San Francisco, CA, ASME, San Francisco, 99–105, 1995.

[3] A. Ghadimi, R. Saidur, et al, A review of nanofluids stability properties and characterization in stationary conditions, *Int. J. Heat and Mass*, **54**, 4051-4068, 2013.

[4] R. D. Deegan, O. Bakajin et al, *Nature*, **389**, 827-829, 1997.

[5] G. M. Whitesides and B. Grzybowski, *Science*, **295**, 2418-2421, 2002.

[6] L. Jiang, L. Gao, and J. Sun, Production of aqueous colloidal dispersions of carbon nanotubes, *J. Colloid Interface Sci.*, **260**, 1, 89–94, 2003.

[7] L. Vandsburger, Synthesis and Covalent Surface Modification of Carbon Nanotubes for Preparation of Stabilized Nanofluid Suspensions, M.Eng., McGill University (Canada), Canada, 2009.

[8] X.-J. Wang and X.-F. Li, Influence of pH on nanofluids' viscosity and thermal conductivity, *Chin. Phys. Lett.*, **26**, 056601, 2009.

[9] M.-S. Liu, M.C.-C. Lin, et al, Enhancement of thermal conductivity with Cu for nanofluids using chemical reduction method, *Int. J. Heat Mass Transfer*, **49**, 3028, 2006.

[10] K.S. Hong, T.K. Hong, et al, Thermal conductivity of Fe nanofluids depending on the cluster size of nanoparticles, *Appl. Phys. Lett.*, **88**, 1, 2006.

[11] H. Zhu, C. Zhang et al, Preparation and thermal conductivity of suspensions of graphite nanoparticles, *Carbon*, **45**, 226, 2007.

[12] C. H. Chun, S. W. Paik et al, Effect of Nanoparticle Sizes and Number Densities on the Evaporation and Dryout Characteristics for Strongly Pinned Nanofluid Droplets, *Langmuir*, **23**, 2953, 2007.

[13] I. Kim and K. Kihm, Progressive dryout of nanofluids on the hydrophilic and hydrophobic surfaces, *Journal of Heat Transfer*, **135**, 080911, 2013.

[14] I. Kim and K.D. Kihm, Hidden cavity formations by nanocrystalline self-assembly on various substrates with different hydrophobicities, *Langmuir*, **28**, 9195, 2012.

[15] K. Kihm, S. S. Cheon, J. S. Park, J. S. Lee, I. Kim, and H. J. Yi, Surface Plasmon resonance (SPR) reflectance imaging: Far-field recognition of near-field phenomena, *Optics and Laser in Engineering*, **50**, 64-73, 2012.

[16] I. Kim and K. D. Kihm, Measuring near-field nanoparticle concentration fields by correlating SPR reflectance with nanofluidic effective refractive index (ERI), *Optics Letters* **35**, 393-395, 2010.

[17] I. Kim and K. D. Kim, Unveiling hidden complex cavities formed during nanocrystalline self assembly, *Langmuir* **25**, 1881-1884, 2009.

[18] I. Kim and K.D. Kihm, Label-Free Visualization of Microfluidic Mixture Concentration Fields Using a Surface Plasmon Resonance (SPR) Imaging, *Exp. In, Fluids*, **41**, 905, 2006.

[19] Raether, H. Surface Plasmons; Springer-Verlag; Berlin, 1988.

[20] Kihm, K. D.; Pratt, D. M. *J. Heat Trans.*, Heat Transfer Gallery, **121**, 1999.

[21] I. Kim, S. Bender et al, Metal Nanoparticle Plasmon-Enhanced Light-Harvesting in a Photosystem I Thin Film, *Nano Letters*, **11**, 3091, 2011

[22] H. Yi, I. Kim, and K. Kihm, Dryout Patterns of Nanofluids With Different Initial Concentrations of Nanoparticles (47nm, Al2O3), *J. of Heat Transfer*, **135**, 080910, 2013.

[23] J. Malicka, I. Gryczynski, et al, Use of Surface Plasmon-Coupled Emission to Measure DNA Hybridization, *J. Biomol. Screen*. **9**, 208, 2009.

[24] L. Laplatine, L. Leroy, et al, Spatial resolution in prism-based surface plasmon resonance microscopy, *Opt. Express*, **22**,22771, 2014.